

PACS numbers: 42.55.Lt; 42.60.Lh
DOI: 10.1070/QE2005v035n04ABEH002867

Compact 4-kHz XeF laser with a multisectional discharge gap

A.V. Andramanov, S.A. Kabaev, B.V. Lazhintsev, V.A. Nor-Arevyan, V.D. Selemir

Abstract. **A XeF electric-discharge laser with a pulse repetition rate f of up to 4 kHz is developed. The laser electrode unit is based on plate electrodes with inductive – capacitive discharge stabilisation. He and Ne are used as buffer gases, and NF_3 serves as a fluorine donor. A narrow ($\sim$1 mm) discharge is achieved; the specific energy deposition per unit length of the active volume is as high as 2 J m^{-1}. The maximum energy in a laser pulse is $\sim$3 mJ for $NF_3-Xe-He$ and $NF_3-Xe-Ne$ mixtures at total pressures of 0.8 and 1.2 atm, respectively, and the maximum lasing efficiency is $\sim$0.73 %. The maximum gas velocity in the working gap is 19 m s^{-1}. The laser-pulse energy at a high pulse repetition rate (4 kHz) virtually coincides with that obtained at a low repetition rate. The mean output pulse power at $f = 4$ kHz reaches 12 W, and the rms deviation of the laser-pulse energy is $\sim$2.5 %.**

Keywords*: electric-discharge XeF laser, plate electrodes, inductive – capacitive stabilisation, pulse repetition rate, stability of laser pulses.*

1. Introduction

Excimer lasers with high (a few kilohertz) pulse repetition rates required for technological applications have been intensively developed in recent years [1 – 3]. In these works, such repetition rates were achieved by narrowing the discharge to several millimetres in the direction of the gas flow. As a result, at a gas circulation velocity $V_g \approx 55$ m s^{-1} in a XeF laser, the pulse repetition rate $f = 5.5$ kHz was obtained in [1]. For a discharge volume of $550 \times 14 \times 2.8$ mm, the best lasing characteristics were achieved in [1] with a $F_2 : Xe : Ne = 3.2 : 16 : 2700$ mbar gaseous mixture and a 4.6-nF capacitive storage. The mean output power was 35 W, and the energy deposition per unit length of the active volume was $\sim$1.5 J m^{-1}.

Therefore, to obtain high pulse repetition rates, it was proposed in [4 – 6] to produce a discharge with a minimum possible width by using plate electrodes. In these works, it was also proposed for the first time to use a multisectional discharge gap jointly with inductive – capacitive discharge stabilisation for producing a stable discharge in the active medium of an electric-discharge laser. The pulse repetition rate achieved in [6] for a nitrogen laser without gaseous-mixture circulation was $>$ 200 Hz. The laser-beam width in the near-field zone was $\sim$1.3 mm.

The aim of this work is the development of a compact excimer laser on the basis of a new electrode unit with a pulse repetition rate of several kilohertz at a gaseous-mixture circulation velocity of 19 m s^{-1}. The laser uses a plate-electrode unit and inductive – capacitive discharge stabilisation.

A.V. Andramanov, S.A. Kabaev, B.V. Lazhintsev, V.A. Nor-Arevyan, V.D. Selemir All-Russian Scientific Research Institute of Experimental Physics – Federal Nuclear Center, prosp. Mira 37, 607188 Sarov, Nizhni Novgorod region, Russia; e-mail: mailbox@ntc.vniief.ru

Received 16 September 2004; revision received 6 December 2004
Kvantovaya Elektronika **35** (4) 311 – 315 (2005)
Translated by A.S. Seferov

2. Experimental results

A flow-type XeF laser was developed on the basis of the working chamber of a commercial CL-5000 excimer laser (Centre of Physical Instrument Making, General Physics Institute, RAS, Troitsk) and a new electrode unit with a multisectional discharge gap. The length and the inner diameter of the chamber's aluminium housing were 430 and 175 mm, respectively. The resonator mirrors ($R_1 = 100$ %, $R_2 = 30$ %) were attached to the chamber end flanges; the distance between the mirrors was 50 cm. A diametrical fan with a wheel 60 mm in diameter, which was rotated by a dc electric motor with a power of 80 W using a magnetic clutch, and a water-cooled heat exchanger were placed inside the chamber. In its upper part, the electrode unit and a laser pump source were arranged.

The discharge gap was formed by 25 pairs of anode and cathode plates oriented in a vertical plane passing through the laser optical axis. The height and total length of the discharge gap were 12 and 260 mm, respectively. The gap was preionised with 25 spark discharges on one side of the discharge gap (downstream of the gas flow).

The laser pulse pump system contained a storage capacitor C_s (3.3 nF), a peaking capacitor C_p (2.35 nF), and a preionisation capacitor C_{pr} (0.5 nF). The laser was powered from a pulsed source (CPIM GPI RAS). The storage capacitor was charged in a time of 240 μs using a resonance diode charging unit (the filtering capacitance was 0.22 μF). The parameters of this unit determined the limiting pulse repetition rate (4 kHz). The peaking capacitor was charged through a two-loop circuit ($C-C$) upon switching the storage capacitor by a TGI-1000/25 thyratron. The inductive – capacitive decoupling was effected by connecting an individual peaking capacitor $C_p^i = 0.094$ nF to each pair of plate electrodes. When a certain voltage was

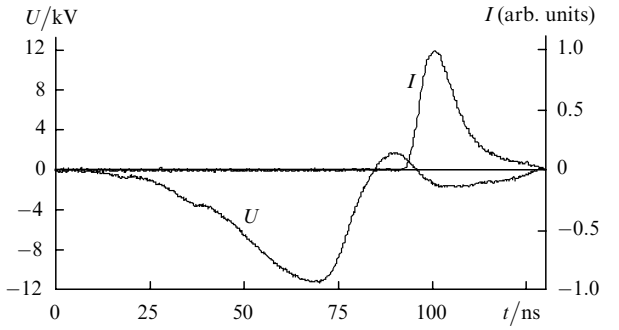

Figure 1. Voltage pulse across the peaking capacitor and a laser intensity pulse at a charging voltage of 18 kV for the $NF_3 : Xe : He = 3 : 6 : 600$-Torr mixture.

reached across the peaking capacitors, the spark gaps of the preioniser were broken down and the charging of its capacitance was initiated.

A $He(Ne)-Xe-NF_3$ active medium was used in our experiments. The maximum total pressure of the active medium was 1.2 atm. Figure 1 shows typical oscillograms of a voltage pulse across the peaking capacitor and a laser pulse for He as the buffer gas. The voltage-pulse rise time is $\sim$40 ns, and its amplitude is 11.4 kV. The laser-pulse duration (FWHM) is $\sim$12 ns. When the charging voltage of the storage capacitor falls to 16 kV, the voltage amplitude across the peaking capacitor remains virtually constant.

Figure 2 shows the optical layout of the experiments for studying the XeF-laser parameters. The distribution profile of the specific energy deposition over the active-volume cross section was determined from the discharge emission in the visible spectral region. The discharge-emission was detected with an Olympus C-4040Zoom digital camera. Laser radiation was removed by misaligning resonator mirrors (*3*) and (*6*) and using light filter (*2*). To increase the depth of focus, photographing was performed in parallel rays using lens (*4*) with a focal length of 1000 mm; its focal plane was at the centre of the discharge gap. The camera objective lens was focused to infinity. A typical photograph of the discharge emission is shown in Fig. 3a. The integrated light-intensity distribution over the height and the light-intensity distribution over the discharge width are shown in Figs 3b and 3c, respectively.

The discharge width defined as the FWHM of the light intensity distribution is 1.1 mm (Fig. 3c). Note that the measured discharge width is somewhat larger than its actual width due to an inaccuracy in installing the electrode plates, which are actually not coplanar. As a result, plasma regions arising between anode–cathode pairs are shifted relative to one another in the discharge-gap width. The small discharge

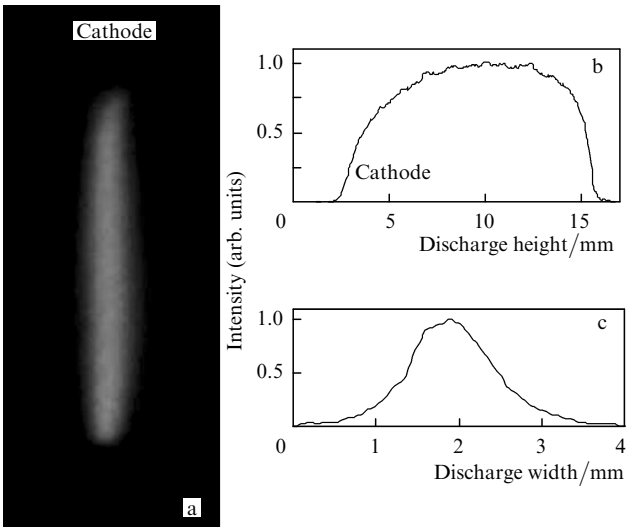

Figure 3. (a) Photograph of discharge emission, (b) the integrated emission intensity distribution over the discharge height, and (c) the emission intensity distribution over its width.

width obtained ($\sim$1 mm) is of interest for achieving ultimately high pulse repetition rates in electric-discharge lasers with a transverse gaseous-mixture flow.

The energy of a single radiation pulse in the mode of a low pulse repetition rate ($f \leqslant 20$ Hz) was measured using ORIEL No. 70271 pyroelectric calorimeter (*8*) (Fig. 2). The energy of a laser-pulse packet (several dozen or hundred pulses) at a high repetition rate ($f \geqslant 1$ kHz) was measured using either ORIEL No. 70263 thermocouple calorimeter (*9*) with a time constant of 2.5 s or an IMO-2 calorimeter with a time constant of 5 s.

It was ascertained that the optimum NF_3 pressure was 2.5–3.5 Torr. In subsequent experiments, the NF_3 pressure was 3 Torr, and the pressures of Xe and buffer gas (He or Ne) were varied. The energy of radiation pulses was measured at $f = 20$ Hz. The results of these experiments are shown in Fig. 4.

The maximum output energy E for mixtures with He and Ne buffer gases was virtually the same and equal to $\sim$3 mJ; the maximum efficiency relative to the energy accumulated in the storage capacitor was $\sim$0.57%. The optimum pressure for the He-based mixtures studied ranged from 0.7 to 0.9 atm; for Ne-based mixtures, the lasing energy increased with pressure to $P = 1.2$ atm. The higher optimum pressure of Ne in the active medium is evidently related mainly to the lower electric strength for Ne (the breakdown voltage in Ne is lower than in He). This results

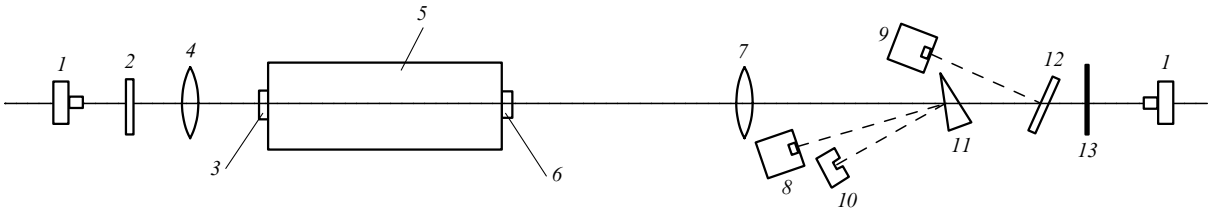

Figure 2. Layout of the experiments on studying the parameters of the XeF laser: (*1*) digital camera; (*2*) light filter; (*3*) highly reflecting mirror; (*4*, *7*) lenses; (*5*) laser chamber; (*6*) output mirror; (*8*) pyroelectric calorimeter; (*9*) thermocouple calorimeter; (*10*) PIM-M energy meter; (*11*) optical wedge; (*12*) beamsplitter; and (*13*) phosphor screen.

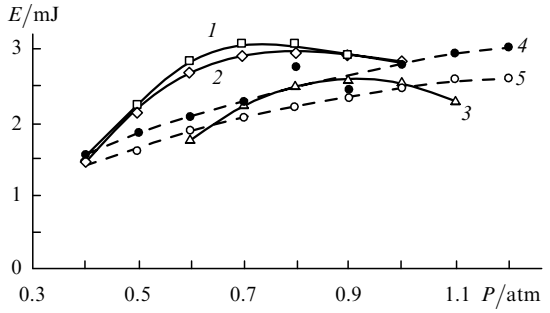

Figure 4. Output energy E as a function of the total pressure of (*1*, *2*, *3*) NF_3–Xe–He and (*4*, *5*) NF_3–Xe–Ne mixtures; the pressure of NF_3 is 3 Torr, Xe–(*1*) 7.5 Torr, (*2*, *4*) 9 Torr, and (*3*, *5*) 6 Torr; the charging voltage of the storage capacitor is 18 kV.

in a higher pressure of Ne required for the peaking capacitor to be charged to the same voltage. The optimum experimental pressure of Xe was 7.5–9 Torr [curves (*1*) and (*2*) in Fig. 4].

Figure 5 shows the XeF-laser output energy E and efficiency η as functions of the charging voltage U. The output energy increases with the charging voltage, being accompanied by a slight decrease in the efficiency. The maximum efficiency (0.73 %) is observed at a charging voltage of 14 kV [curves (*4*) and (*6*)]. In an NF_3 : Xe : Ne mixture with an increased Ne content [curve (*5*)], the maximum efficiency (0.66 %) is observed at a charging voltage of 16 kV.

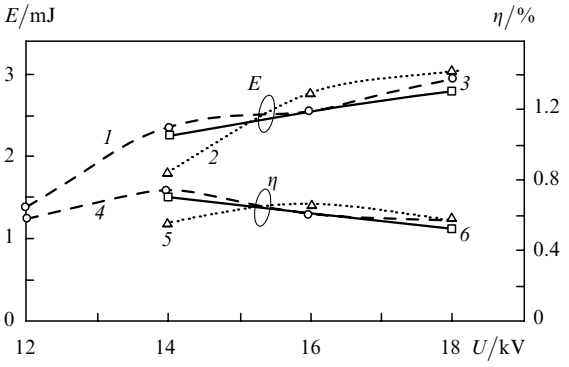

Figure 5. Output energy E (*1*, *2*, *3*) and XeF-laser efficiency η (*4*, *5*, *6*) as functions of the charging voltage U for (*1*, *4*) NF_3 : Xe : He = 3 : 9 : 600 Torr, (*2*, *5*) NF_3 : Xe : Ne = 3 : 9 : 900 Torr, and (*3*, *6*) NF_3 : Xe : Ne = 3 : 9 : 770 Torr mixtures.

A decrease in the efficiency with increasing the charging voltage is probably associated with a high specific pump power. The specific energy deposition in the 1-mm wide active medium at a charging voltage of 18 kV was $\sim$0.09 J cm^{-3} ($\sim$0.11 J cm^{-3} atm^{-1} for a He-based mixture), and the specific pump power was 9 MW cm^{-3}. These values are much higher than the specific energy depositions and pump powers ($\sim$0.03 J cm^{-3}, 0.011 J cm^{-3} atm^{-1}, and 3 MW cm^{-3}) achieved in [1]. A decrease in the XeF-laser efficiency at a specific pump power of >5 MW cm^{-3} was observed in [1]. An increase in the laser efficiency with a decrease in the charging voltage can partially be associated with the fact that a greater part of energy stored in the storage capacitor is transferred to the peaking capacitor before a breakdown of the discharge gap.

The maximum output energy for Ne and He mixtures was 3 mJ, and the maximum efficiency at a charging voltage of 14 kV was 0.73 %. A further increase in the maximum efficiency of the XeF laser can be expected when using a stable resonator with a spherical mirror, in which the diffraction loss falls for narrow ($\sim$1 mm) discharges, and with an increase in the discharge-gap length and, correspondingly, in the resonator filling factor. In fact, when a spherical Al mirror with a 4-m radius of curvature of the reflecting surface was used as the highly reflecting mirror, the output energy increased by 10 %. Optimising the preionisation system in both the spark-initiation moment and the electric-capacitance value is also required.

At the next stage of this work, we studied the laser operation in a repetitively pulsed mode. Figure 6 shows the energy of a laser-pulse packet (the first 100 pulses) as a function of the pulse repetition rate. As f increases to 2 kHz, the energy of the pulse packet rises for a He-based active mixture; the efficiency correspondingly increases from 0.57 % to 0.61 % [curve (*1*)]. As f increases to 4 kHz, the efficiency decreases to 0.55 %, which is close to the lasing efficiency in the mode of a low pulse repetition rate.

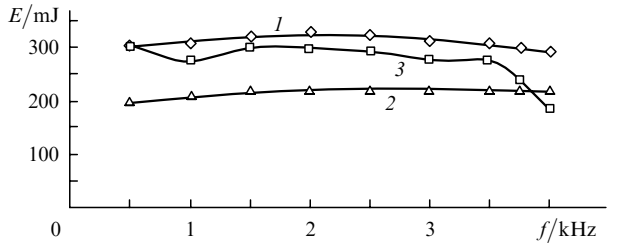

Figure 6. Output energy E of a packet of 100 laser pulses as a function of the pulse repetition rate f for (*1*, *2*) NF_3 : Xe : He = 3 : 9 : 600 Torr and (*3*) NF_3 : Xe : Ne = 3 : 9 : 760 Torr mixtures at charging voltages of the storage capacitor of (*1*, *3*) 18 and (*2*) 14 kV.

When the charging voltage of the storage capacitor falls to 14 kV [curve (*2*) in Fig. 6], the lasing efficiency increases from 0.61 % (for $f = 500$ Hz) to 0.69 % (3.5 kHz). At $f = 4$ kHz, the lasing efficiency is 0.67 %, which is $\sim$1.2 times higher than at a charging voltage of 18 kV [curve (*1*) in Fig. 6]. For a Ne-based active mixture (at a total pressure of 1 atm) at frequencies of 1.5–3.5 kHz, the energy of a pulse packet and the lasing efficiency fall slightly [curve (*3*) in Fig. 6]. At $f = 4$ kHz, the lasing efficiency falls abruptly (by a factor of $\sim$1.5). As the voltage across the storage capacitor falls to 14 kV, the lasing efficiency for this mixture falls in the same manner, and, as the total pressure of Ne rises to 1.2 atm, the efficiency begins to fall at $f = 3$ kHz. This can be explained by a reduced gas velocity in the discharge gap, since the fan is unable to hold it with an increase in the Ne pressure.

Therefore, at a high pulse repetition rate, it is desirable to use a He-based active mixture. At $f = 4$ kHz, the maximum mean lasing power was 11.7 W.

The energy of laser pulses as a function of their repetition rate was measured with a PIM-M energy meter connected to a PC (Fig. 2). The energy was measured in arbitary units at $f \leqslant 5$ kHz. The maximum number of pulses that could be measured with this device was 1000. The data on the energy of each pulse in a packet is automatically transmitted from the PIM-M to the PC. For each packet

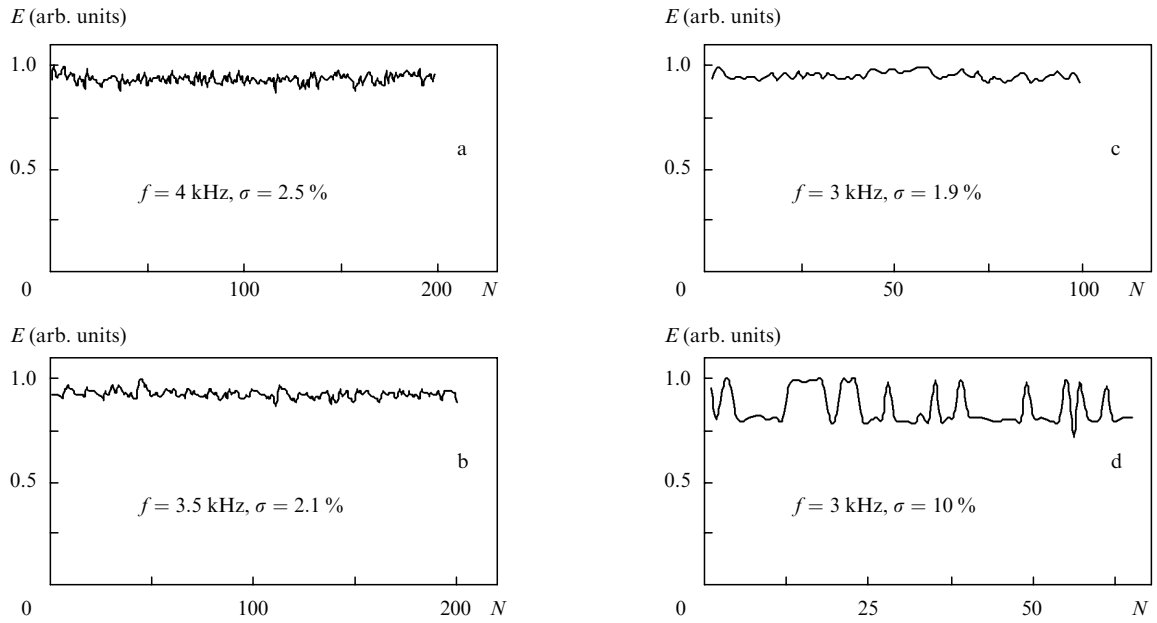

Figure 7. Energy E of laser pulses as a function of the pulse number N for (a, b, d) $NF_3 : Xe : Ne : He = 3 : 7.5 : 76 : 520$ Torr and (c) $NF_3 : Xe : Ne = 3 : 9 : 900$ Torr mixtures at a charging voltage of the storage capacitor of 18 kV.

that usually contained several hundred pulses, the dependence of the output pulse energy on the pulse number was plotted and the rms deviation σ of the laser-pulse energy was calculated.

Figure 7 shows the results from measuring the stability of the output pulse energy in the range 3–4 kHz. The best stability of the pulse energy ($\sigma = 2.5\,\%$) for $f = 4$ kHz is achieved for the $NF_3 : Xe : Ne : He = 3 : 7.5 : 76 : 520$ Torr mixture (Fig. 7a). A small admixture of Ne improves the energy stability of laser pulses. When the pulse repetition rate falls to 3.5 kHz, the stability improves ($\sigma = 2.1\,\%$, Fig. 7b). For a Ne-based mixture, the rms deviation of the output pulse energy is 1.9 % at $f = 3$ kHz (Fig. 7c). Reducing the gas-flow velocity disturbs a stable regime of laser operation and significantly impairs the energy stability of laser pulses ($\sigma = 10\,\%$, Fig. 7d).

Figure 8 presents the near- and far-field distributions of the output-energy density J over the laser-beam cross section. Laser radiation was visualised using a phosphor screen (Fig. 2), the emission from which was photographed by the digital camera. To record the near-field distribution of laser radiation, an image of the central region of the discharge gap was formed using a lens, thereby helping to determine the lasing region more accurately without distortions caused by a beam divergence. Figures 8a and 8b show the distribution of the output-energy density over the beam width and the integral distribution of the energy density over the beam height, respectively. Typical beam width and height are 1×12 mm. Thus, the laser-beam width in the near-field zone is ~ 1 mm, which is 2–3 times less than in the XeF laser considered in [1].

The far-field radiation of the laser with a spherical mirror with $R_1 = 100\,\%$ was recorded by placing the phosphor screen in the focal plane of a lens with a 2131-mm focal length. Figures 8c and 8d show the horizontal and integral vertical distributions of the energy density, respec-

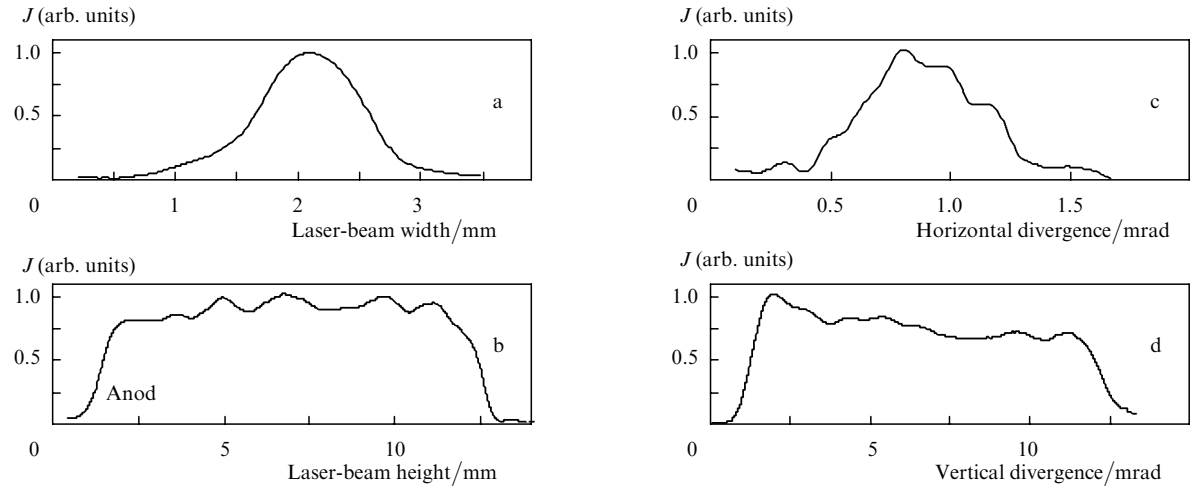

Figure 8. Near-field distribution of the output-energy density J over the beam cross section for (a, b) a parallel-plate resonator and (c, d) far-field distribution for a resonator with a spherical mirror.

tively. The divergence of laser radiation at a halved-intensity level was 0.6×10 mrad.

3. Conclusions

This study has shown that the use of plate electrodes allows the formation of a narrow discharge, resulting in a high pulse repetition rate at a comparatively low gas-flow velocity and a low power (80 W) expended on the gas-flow production. The high energy stability of laser pulses ($\sigma = 2\,\% - 2.5\,\%$) is largely achieved due to inductive–capacitive discharge stabilisation. The energy stability of laser pulses can be further increased by improving both the accuracy of setting the electrode plates and the shape of their working surface, increasing the length and height of the discharge gap, improving the stability of the laser power supply, optimising the resonator, etc.

Further optimisation of the laser parameters and use of a choke with a lower inductance in the circuit of resonance diode charging of the storage capacitor allowed the pulse repetition rate to be raised to 5 kHz. At a charging voltage of 14 kV and $f = 5$ kHz, the mean XeF-laser output power is 11.5 W and the efficiency is 0.71 %.

References

1. Borisov V.M., Vinokhodov A.Yu., Vodchits V.A., El'tsov A.V. *Kvantovaya Elektron.*, **30**, 881 (2000) [*Quantum Electron.*, **30**, 881 (2000)].
2. Myers D., Watson T.A., Das P.P., Partlo W.N., Hofmann T., Padmabandu G.G., Zambon P., Hysham C., Dunning R. *Proc. SPIE Int. Soc. Opt. Eng.*, **3679**, 1038 (1999).
3. Saito T., Sazuki T., Yoshino M., Wakabagashi O., Matsunaga T., Fujimoto J., Kakizaki K., Yamazaki T., Inoue T., Terashima K., Enami T., Inoue H., Sumitani A., Tomaru H., Mizoguchi H. *Proc. SPIE Int. Soc. Opt. Eng.*, **5040**, 1704 (2003).
4. Lazhintsev B.V., Nor-Arevyan V.A. RF Patent No. 2089981, 5 January 1996; *Byull. Izobret.*, (25), 355 (1996).
5. Lazhintsev B.V., Nor-Arevyan V.A. *Kvantovaya Elektron.*, **30**, 3 (2000) [*Quantum Electron.*, **30**, 3 (2000)].
6. Andramanov A.V., Kabaev S.A., Lazhintsev B.V., Nor-Arevyan V.A., Selemir V.D. *Proc. SPIE Int. Soc. Opt. Eng.*, **4747**, 64 (2002).